Unsteady nonlinear free surface flows around an oscillating hydrofoil

M. Landrini *C. Lugni* *V. Bertram*
INSEAN, Italian ship model basin, Roma – Italy.

A model is under development to study the hydrodynamics of a flapping foil $\mathcal{H}$ beneath water waves. Cavitation effects and large separation phenomena are ruled out but nonlinearities due to moving and free boundaries are fully retained. In this framework, the flow field, sketched in fig. 1, can be qualitatively described in terms of inviscid–rotational fluid mechanics in which a thin vortical layer mimics the hydrofoil wake $\mathcal{W}$. A suitable unsteady Kutta condition provides the mechanism for vorticity generation. A possible approach for solving the

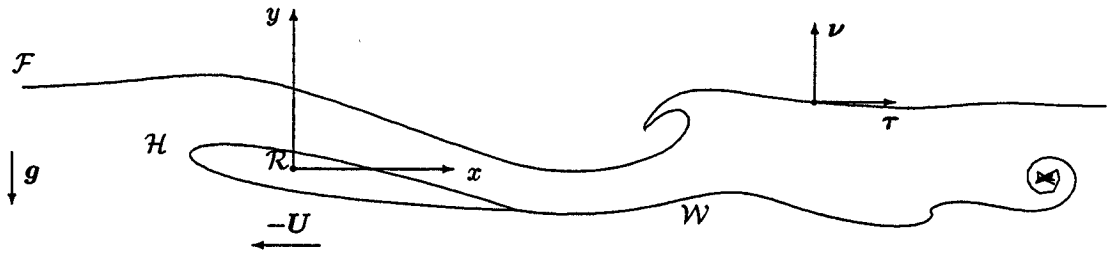

Figure 1: Definition sketch.

problem consists in splitting the kinetics and the dynamics of the phenomenon. The velocity field $\boldsymbol{u}$, in facts, satisfies the purely kinematic problem

$$\nabla \cdot \boldsymbol{u} = 0 \qquad \nabla \times \boldsymbol{u} = \gamma_{\mathcal{W}} \tag{1}$$

which can be solved, for fixed time t, provided enough boundary data are available. $\gamma_{\mathcal{W}}$ is the generalized vorticity distribution.

The evolution in time of the flow field is given in terms of kinematic and dynamic equations for the free surface $\mathcal{F}$ and the wake $\mathcal{W}$. In particular, the free surface is described by

$$\frac{\partial \boldsymbol{P}(\chi,t)}{\partial t} = \boldsymbol{w} = u_\nu \boldsymbol{\nu} + w_\tau \boldsymbol{\tau} \qquad \frac{\partial u_\tau(\chi,t)}{\partial t} = \boldsymbol{\tau} \cdot \left\{ (\boldsymbol{w}-\boldsymbol{u}) \cdot \nabla \boldsymbol{u} + \boldsymbol{g} - \frac{1}{\rho} \nabla p_a \right\} + \boldsymbol{u} \cdot \frac{\partial \boldsymbol{\tau}(\chi,t)}{\partial t} \tag{2}$$

being $\boldsymbol{P}(\chi,t)$ a generic point on $\mathcal{F}$. $\boldsymbol{\nu}$ and $\boldsymbol{\tau}$ are the unit normal and tangent vectors to $\mathcal{F}$ in $\boldsymbol{P}(\chi,t)$. The first equation states that the point $\boldsymbol{P}$, labeled by χ, moves with a velocity $\boldsymbol{w}$: the normal component $\boldsymbol{w} \cdot \boldsymbol{\nu}$ is fixed by the corresponding component $u_\nu = \boldsymbol{u} \cdot \boldsymbol{\nu}$ of the fluid below, while the tangential one, w_τ, can be arbitrarily chosen. Regardless the actual value of w_τ, the tangential velocity component u_τ of the fluid evolves according to the second equation, which follows by the Euler equation.

The vorticity is assumed confined in a narrow wake $\mathcal{W}$ downstream the hydrofoil and modeled by means of a zero thickness vortex layer of local strength

$$\gamma_{\mathcal{W}} = \gamma_{\mathcal{W}} \boldsymbol{k} = (\boldsymbol{u}_+ - \boldsymbol{u}_-) \times \boldsymbol{\nu} = [u_\tau] \boldsymbol{k} \,,$$

where $[u_\tau]$ is the jump of the tangential velocity across the vortex sheet and $veck = \boldsymbol{\tau} \times \boldsymbol{\nu}$. The point-wise motion of $\mathcal{W}$ is fully described by the system of equations

$$\frac{\partial \boldsymbol{P}(\xi,t)}{\partial t} = \boldsymbol{v}(\xi,t) \qquad \frac{\partial [J \gamma_{\mathcal{W}}](\xi,t)}{\partial t} = 0 \tag{3}$$

In the first equation, $\boldsymbol{P}(\xi,t)$ is the position of a wake point, marked by the particle coordinate ξ, which moves with a velocity defined as $\boldsymbol{v}(\xi,t) = \frac{1}{2}(\boldsymbol{u}_+ + \boldsymbol{u}_-)$. The dynamic equation, where $J(\xi,t) = |\partial \boldsymbol{P}/\partial \xi|$, allows for the time evolution of the concentrated vorticity $\gamma_{\mathcal{W}}(\xi,t)$. The initial value problem for equations (3) is defined by the condition that the wake is continuously shed from the trailing edge with a vorticity density γ_{TE} to be determined according to the assumption of zero trailing edge loading.

The kinetic problem (1) is solved numerically by a boundary element method. The velocity field is expressed by

$$\begin{aligned} \boldsymbol{u}(\boldsymbol{Q}) &= \nabla_Q \int_{\mathcal{F}} \boldsymbol{u}\cdot\boldsymbol{n}\, G\, dS_P + \nabla_Q \times \int_{\mathcal{F}} \boldsymbol{u}\times\boldsymbol{n}\, G\, dS_P \\ &+ \nabla_Q \int_{\mathcal{H}} \sigma\, G\, dS_P + \frac{\Gamma}{\mathcal{L}}\nabla_Q \times \int_{\mathcal{H}} \boldsymbol{k}\, G\, dS_P + \nabla_Q \times \int_{\mathcal{W}} \gamma_{\mathcal{W}}\, G\, dS_P \end{aligned} \tag{4}$$

where $G(\boldsymbol{Q},\boldsymbol{P}) = \ln|\boldsymbol{P}-\boldsymbol{Q}|/2\pi$ is the two dimensional free–space Green function. In (4), the influence of the free surface appears 'directly' in terms of the normal $\boldsymbol{u}\cdot\boldsymbol{n}$ and tangential $\boldsymbol{u}\times\boldsymbol{n}$ velocity components on $\mathcal{F}$, while the body is represented through a source distribution σ superimposed to a uniform vortex sheet with strength related to the instantaneous circulation $\Gamma = \int_{\mathcal{H}} \boldsymbol{u}\cdot\boldsymbol{\tau} d\ell$ around the hydrofoil. Finally, the last contour integral accounts for the rotational thin wake. The above integral representation is still valid for a more general viscous velocity field for which the vorticity is generally spread over a larger area, e.g. [4].

The normal velocity component on $\mathcal{H}$ is explicitly known by the no–penetration condition, while u_τ, Γ and the wake influence are assumed known at time t from the previous history. The still unknown velocity component $\boldsymbol{u}\cdot\boldsymbol{\nu}$ on $\mathcal{F}$ and the source strength σ can be evaluated by solving proper integral equations following from (4). A more detailed description of the numerical aspects is given in [3].

Once the velocity field is computed, the free surface and the wake equations are stepped forward in time by a standard fourth order Runge–Kutta scheme to provide a new set of boundary data.

Upon simulating the start from rest, steady regime results are eventually obtained for a NACA 0012 towed at constant velocity and compared with the celebrated experimental data by Duncan (1983). The overall agreement is satisfactory, cfr. fig. 2, although the depression over the profile tends to be under-predicted. At the smallest d/h, a kind of set down of the experimental profile with respect to the numerical solution is also detected and demands for a deeper insight of the experimental uncertainty too. Consistently with the observed agreement, the drag, computed by pressure integration and shown in fig. 3, compares reasonably well with the experimental data [2].

For $d/c = 0.9507$ the waves are close to breaking: Duncan reported a steady non-breaking profile which, upon perturbing the free surface ahead the foil, became characterized by a steady spilling breaker located at the first wave crest past the foil. In the numerical computation the breaking is triggered by simulating the sudden start of the foil: after $tU/c = 10.9$ a tiny jet develops at the first crest past the body. It is shown in natural scale in the top left frame of fig. 4. Because of the breaking, the computation stops and, due to the limited duration of the simulation, a regular wave train cannot develop, nor are we able to model the post-breaking evolution (a possible way to overcome this difficulty could be the matching with Cointe & Tulin (1994) model). In spite of this, close to the hydrofoil, the non-breaking measurements, ∘, agree well with our unsteady solution. In the same plot, two different numerical solutions of the steady Navier-Stokes equations are reported from [6] which both agree well with the experiments and our solution. In particular, when transition to turbulence in the body boundary layer is modeled, •, a larger peak past the foil is obtained which strikingly resembles the one predicted by our inviscid-rotational unsteady model. Results with a fully developed turbulent boundary layer perform slightly better than the other computations at least close to the hydrofoil. Anyway, further downstream, all the methods suffer phase lag and under-prediction of the wave height with respect to the experimental profile. For viscous computations this could be due to the finite extent of the computational domain. Upon observing the non-uniformity of the measured wave train, it is possible that the experimental data are still largely affected by the transient and that on a suitable time scale the breaking would anyway appear. Numerical simulations of stronger plunging breakers induced by a shallowly submerged hydrofoil are discussed in [5].

Some preliminary results for the unsteady flow around a pitching hydrofoil are shown in fig. 5 for $F_n = 1.2857$ and mean submergence $d/c = 1.2857$. An oscillation amplitude of 5 degrees around a zero incidence has been considered for three different values of the pitching period T which correspond to reduced frequencies $\tau = 2\pi U/gT = 2.035$, 1.0177 and 0.2374. The resulting wave patterns (solid lines) are reported from top down, respectively; the steady wave system for the foil advancing without oscillating is also shown (dashed lines). As it is expected on the ground of linear theory, this lee wave system is still present in the oscillating cases. In particular, for the shortest period (top plot) the dominant radiated wavelength is about the same of the lee wave and the observed amplitude is slightly increased. For this relatively high oscillation frequency, the wake pattern, shown in fig. 6, is quite complex but practically decoupled from the free surface because of the large enough submergence depth.

By doubling the oscillation period, a longer wave (about 5c) is radiated downstream and a more modulated wave pattern is observed. In the third plot a frequency slightly smaller than the critical one is considered and, although in the results shown a steady regime is not reached yet, the presence of large amplitude waves located both downstream and upstream the foil is apparent. An extended set of results and a deeper analysis for the flapping foil problem will be presented at the Workshop.

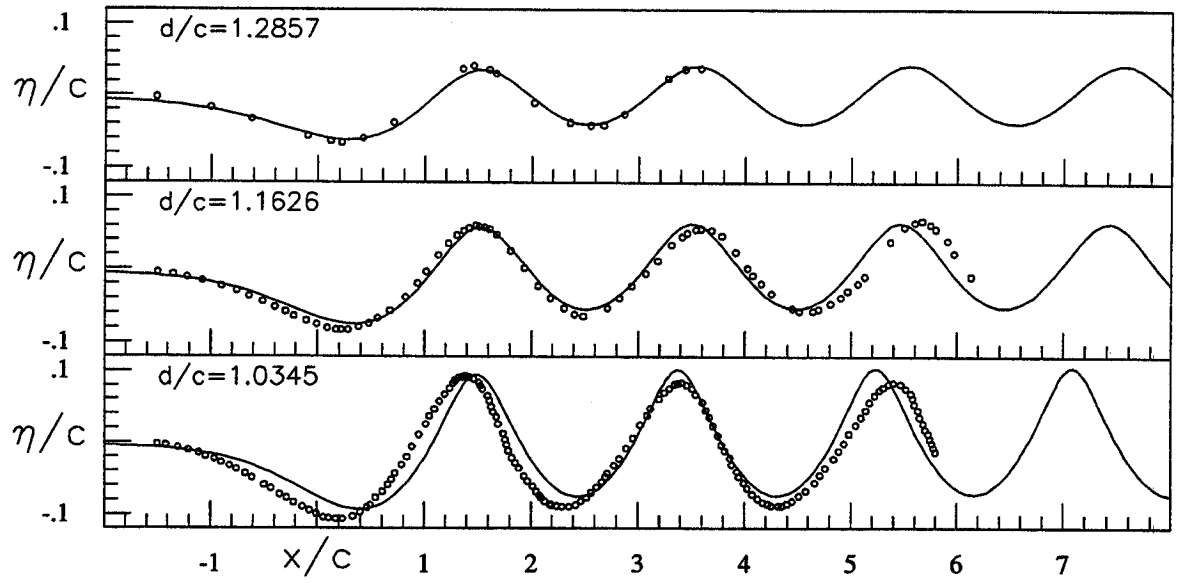

Figure 2: Wave height η past a NACA 0012 ($F_n = U/\sqrt{gc} = 0.567$). From top–down, numerical predictions (solid lines) and Duncan measurements, $\circ$, are contrasted for decreasing submergence depth d. The mid–chord point is located at $(x = 0, y = -d)$ and the incidence is 5 degrees.

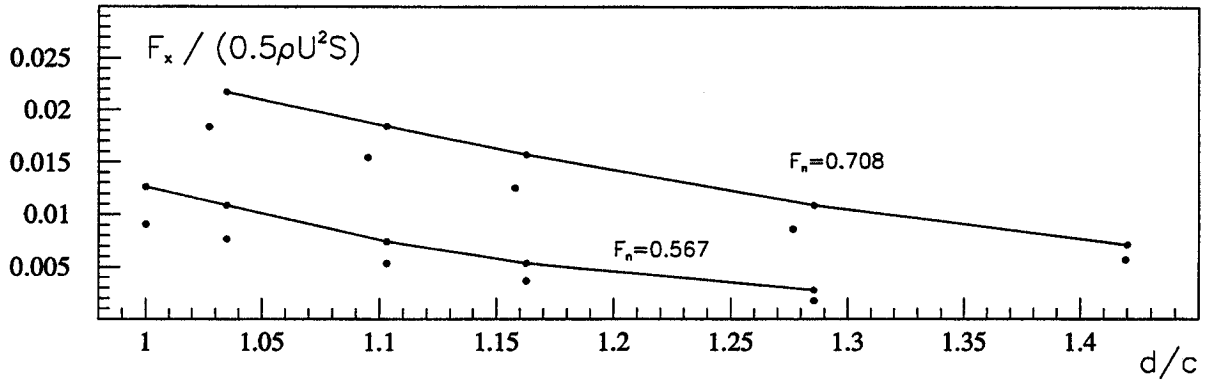

Figure 3: Numerical wave drag for a NACA 0012 ($F_n = 0.567, 0.708$). Symbols are from [2].

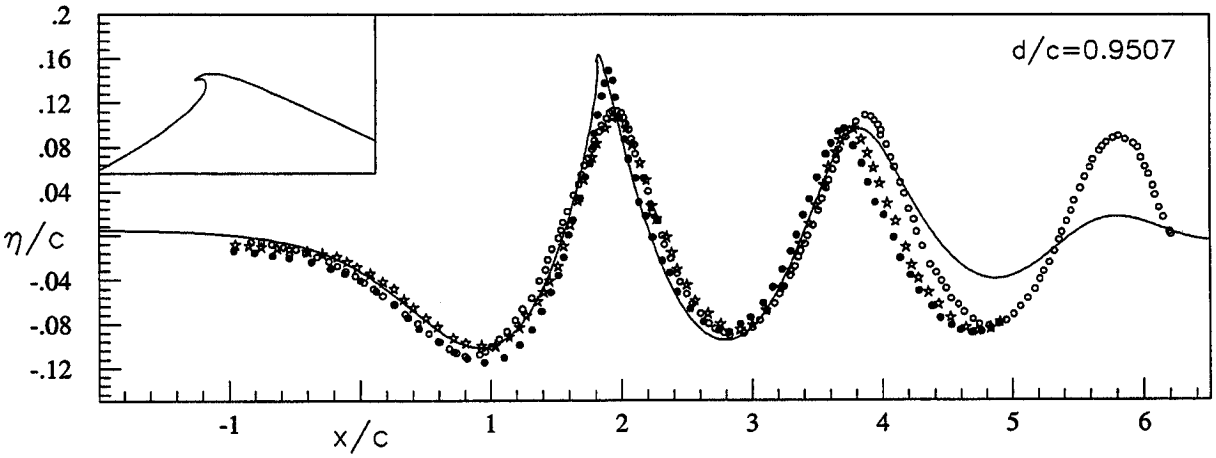

Figure 4: Wave profile η/c past a NACA 0012 ($F_n = 0.5669$, $\alpha = 5°$, $d/c = 0.9507$). Solid line: present unsteady solution at $tU/c = 10.9$; $\circ$: measured 'non-breaking' wave height, [2]; $\star$, $\bullet$: steady Navier-Stokes solutions [6] for fully turbulent and transitional body boundary layer, respectively.

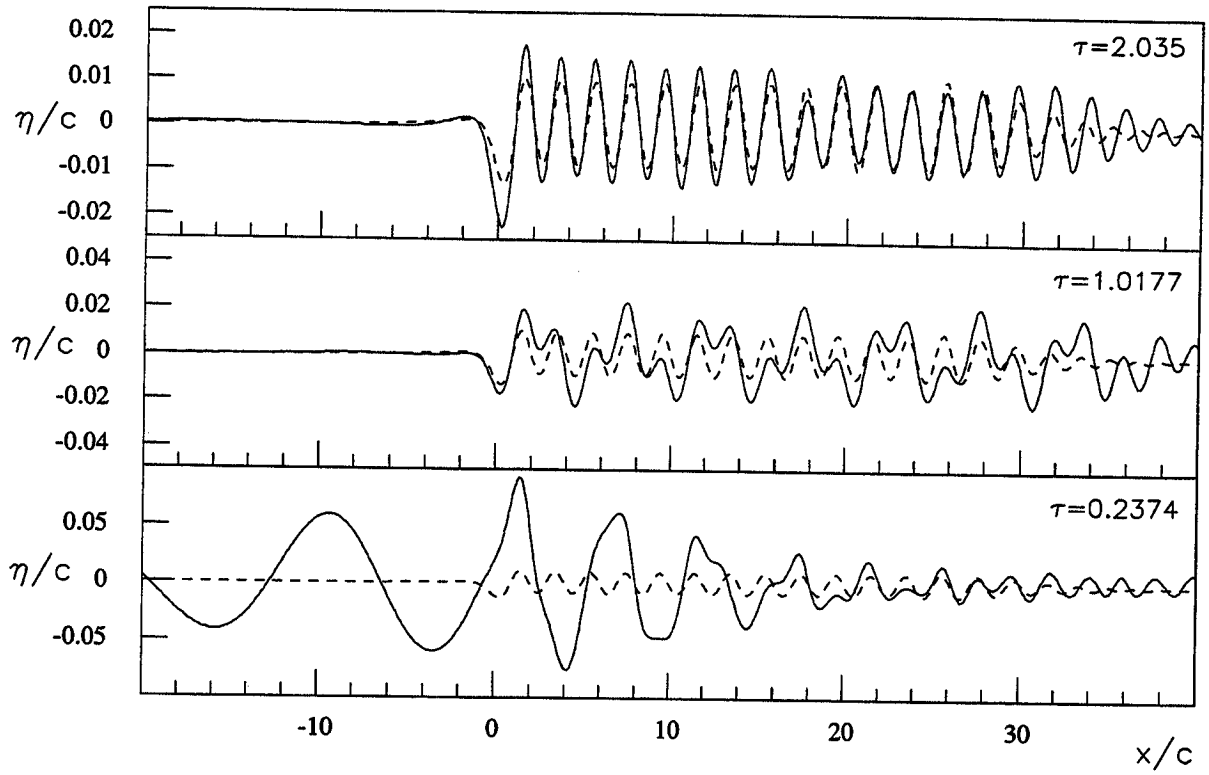

Figure 5: Wave patterns generated by a pitching hydrofoil for decreasing frequency τ ($F_n = 0.5699$). Dashed lines represent the steady wave pattern for fixed hydrofoil.

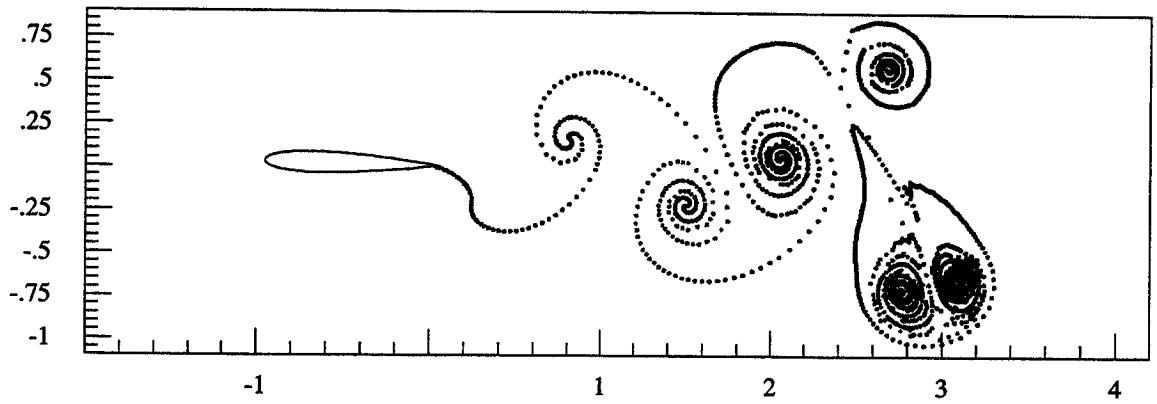

Figure 6: Wake pattern past NACA profile pitching at high reduced frequency.

[1] R. COINTE, M.P. TULIN, (1994). *A theory of steady breakers.* J. Fluid Mech., **276**.

[2] J. DUNCAN, (1983). *The breaking and non-breaking wave resistance of a two dimensional hydrofoil,* J. Fluid Mech. 126.

[3] G. GRAZIANI, M. LANDRINI, (1998). *Application of multipoles expansion technique to two-dimensional nonlinear free surface flows.* to appear in J. Ship Research.

[4] M. LANDRINI, M. RANUCCI, C. M. CASCIOLA AND G. GRAZIANI, (1998). *Viscous effects in wave–body interaction.* Int. J. Off. and Polar Eng..

[5] M. LANDRINI, C. LUGNI, V. BERTRAM, (1999). *Numerical Simulation of the Unsteady Flow Past a Hydrofoil.* to appear in Ship Technology Research.

[6] G.D. TZABIRAS, (1997). *A numerical investigation of 2d, steady free surface flows,* Int. J. Num. Methods in Fluids 25, pp. 567-598